Chip-scale fluorescence microscope based on a silo-filter complementary metal-oxide semiconductor image sensor

Seung Ah Lee,[1,*] Xiaoze Ou,[1] J. Eugene Lee,[2] and Changhuei Yang[1]

[1]*Department of Electrical Engineering, California Institute of Technology, Pasadena, California 91125, USA*

[2]*Center for Bioanalysis, Division of Metrology for Quality of Life, Korea Research Institute of Standards and Science, Daejeon 305-340, South Korea*

**Corresponding author: salee30@caltech.edu*

Received March 13, 2013; accepted April 8, 2013;
posted April 16, 2013 (Doc. ID 186601); published May 21, 2013

We demonstrate a silo-filter (SF) complementary metal-oxide semiconductor (CMOS) image sensor for a chip-scale fluorescence microscope. The extruded pixel design with metal walls between neighboring pixels guides fluorescence emission through the thick absorptive filter to the photodiode of a pixel. Our prototype device achieves 13 μm resolution over a wide field of view (4.8 mm × 4.4 mm). We demonstrate bright-field and fluorescence longitudinal imaging of living cells in a compact, low-cost configuration.

OCIS codes: (110.0180) Microscopy; (180.2520) Fluorescence microscopy.
http://dx.doi.org/10.1364/OL.38.001817

Fluorescence microscopy is a powerful tool for visualizing inter- and intra-cellular dynamics in biological processes. With a wide variety of probes available, fluorescence imaging provides target-specific, high-contrast images suitable for quantitative and automated data analysis. Lens-based epifluorescence microscopes have long been standard equipment in biological imaging despite their inherent disadvantages of high cost, large size, and limited field of view (FOV). A fluorescence imaging system that overcomes these drawbacks can greatly improve the efficiency and the cost of image-based analyses, such as high content screening [1], lineage tracing [2], and migration assays [3].

Low-cost lensless imaging systems using complementary metal-oxide semiconductor (CMOS) image sensors are a good alternative for conventional microscopes [4–8]. Recently, we have reported a chip-scale microscope, named ePetri, designed for long-term monitoring of cells grown on a CMOS imager [5]. The ePetri employs the subpixel sweeping perspective microscopy (SPSM) method, where the light source above the sample is scanned to create subpixel-shifted shadow images, which are reconstructed into a single high-resolution image with the pixel super-resolution algorithm [9]. The ePetri prototype achieved high-resolution (660 nm) bright-field imaging over a wide FOV (6 mm × 4 mm) with a compact, low-cost configuration.

Implementation of fluorescence capability in chip-scale microscopes has been challenging due to the incoherent nature of fluorescence emission and the need for high-performance filters. Absorptive color dyes make good candidate materials for an emission filter thanks to their low cost and ease of fabrication. However, the limited absorptive property of dyes necessitates a substantially thick filter layer, which imposes a separation between the sample and the detector. As a result, the fluorescence emission would spread over multiple pixels and degrade the imaging resolution. Previous works have used a fiber guide plate to confine the fluorescence collection angle, but the achieved resolution of approximately 100 μm [based on the point spread function (PSF)] is restrictive for bio-imaging applications where higher resolution is strongly desired [7,8]. A chip-scale fluorescence imaging solution with a resolution of approximately 10 μm (defined through the PSF) is sought but has so far eluded practical implementation.

We developed a lensless fluorescence microscope using a CMOS image sensor with a silo-filter (SF) lattice structure. SFs with metal walls isolating each pixel can guide fluorescent light through the thick absorptive filter layer and onto the photodiode of a single pixel in the image sensor. This structure relays the plane of highest acuity from the sensor's surface to the top of the filter. We successfully fabricated such a structure on a working CMOS image sensor and obtained wide-field (4.8 mm × 4.4 mm) fluorescence imaging with 13 μm resolution. In combination with the SPSM method, we can perform transmission bright-field imaging and target-specific fluorescence imaging on a single ePetri platform.

The imaging system consisted of a CMOS camera with an SF image sensor and the light sources for fluorescence excitation and SPSM imaging. The target sample, such as living cells, was placed on the surface of the SF sensor. Two modes of imaging are available: bright-field imaging by the SPSM method using 8 × 8 red light-emitting diode (LED) array illumination (625 nm, 5 μW/cm^2 per LED), and fluorescence imaging exploiting a high-power green

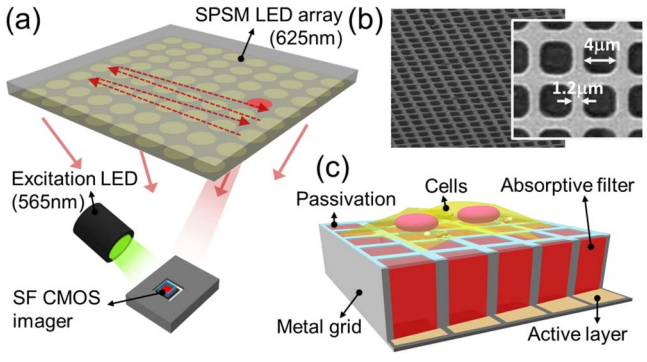

Fig. 1. (a) Schematic diagram of bright-field and fluorescence imaging system using a SF imager. (b) SEM micrograph of metal grid structure. (c) Schematic diagram of the SF structure.

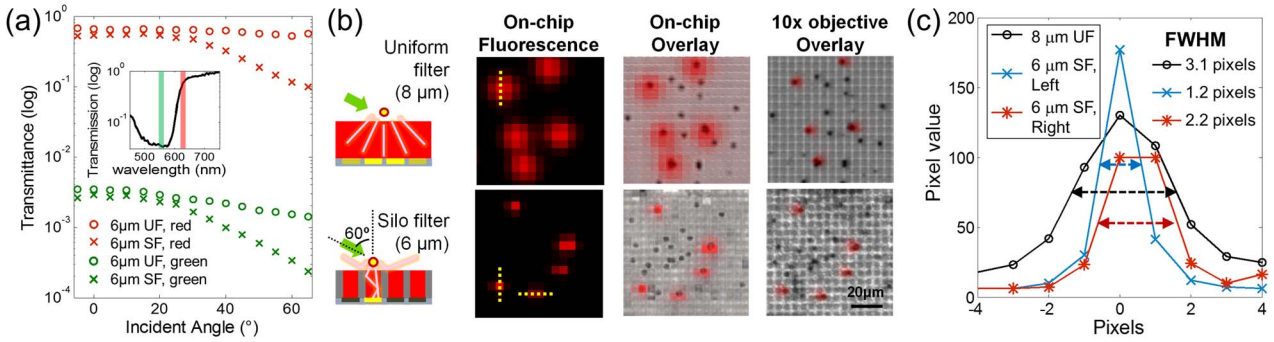

Fig. 2. (a) Transmission of light at varying incidence angles for uniform filter (UF) and silo-filter (SF) with 560 nm (green) and 625 nm (red) plane wave illumination. The transmission curve of the Orasol Red filter (3 μm) is shown (inset). (b) Bright-field and fluorescent images of fluorescent and non-fluorescent microbeads in UF and SF sensors (Full-field image available at Media 1). Results are confirmed with 10× objective microscope images. (c) PSFs of fluorescent microbeads from (b).

LED with a Texas Red excitation filter (559±34 nm, 1 mW/cm^2). For bright-field imaging, we scanned the LED array to obtain 64 low-resolution images (15 ms exposure), which were combined into a high-resolution image aided by pixel super-resolution reconstruction [5,9]. Fluorescence images were taken with the excitation beam incident at a 60° angle [Fig. 1(a)]. The integration time ranged from 100 to 450 ms. The total imaging time was approximately 40 s, which included delays in device control and data transfer. The size of the entire system was 15 cm × 15 cm × 15 cm. We performed all cell culture experiments inside a commercial CO_2 incubator.

The pixel structure of an SF sensor is depicted in Fig. 1(c). The SF structure introduces pixelation in the filter layer with the metal grid blocking light crosstalk between pixels. As a result, fluorescence emission is confined to the pixel that is directly underneath the fluorophore. The prototype SF sensor was fabricated on a commercial CMOS image sensor (5.2 μm, 1024 × 1256 pixels). We first built the metal walls aligned with the sensor's pixel grid by nickel electroplating over an SU-8 photoresist mold. After removing the mold, holes were filled with the Orasol Red absorptive red pigment. The top surface of the structure was coated with a polystyrene passivation layer for cell culture. The Orasol Red longpass filter has a 590 nm cutoff, appropriate for detecting red to far-red dyes with green excitation. The prototype had an SF-metal grid structure of 6 μm height and 4 μm opening with 1.2 μm metal walls, achieving a 59% filter fill factor [Fig. 1(b)].

Figure 2(a) shows the angular sensitivity of the SF to the plane illumination light field at 560 nm and 625 nm (nominal excitation and emission wavelengths of Texas Red). We measured light transmission at varying angles of incidence through a uniform filter (UF) and SF of the same height. In the case of a UF, transmittance at a large incident angle is reduced due to the increased light traveling distance through the absorptive layer. With an SF, this loss is enhanced further due to scattering from the metal surface and the imperfect reflectance of the metal wall (~65% at 590 nm [10]). As a result, we can achieve a comparable background rejection with a thinner SF structure than the UF. At 60° incidence for the excitation beam at 560 nm, a 6 μm SF filter provided 3.8 optical density units, suitable for fluorescence imaging.

The SF sensor sacrifices a large-angle component of the fluorescence emission due to the metal grid. The angular transmission data from Fig. 2(a) at 625 nm provide a means for estimating that the fraction of isotropic fluorescence emission that can be effectively measured by the sensor is approximately 6%. This collection efficiency of the SF sensors can be improved by increasing the fill factor, optimizing the absorptive dye, and improving the surface uniformity and reflectance of the metal grid.

We first verified the fluorescence detection capability of our prototype by imaging fluorescent microspheres on the UF and SF sensors. A mixture of Texas Red fluorescent polystyrene microspheres (2.5 μm) and nonfluorescent microspheres (2 μm) were placed on the surface of

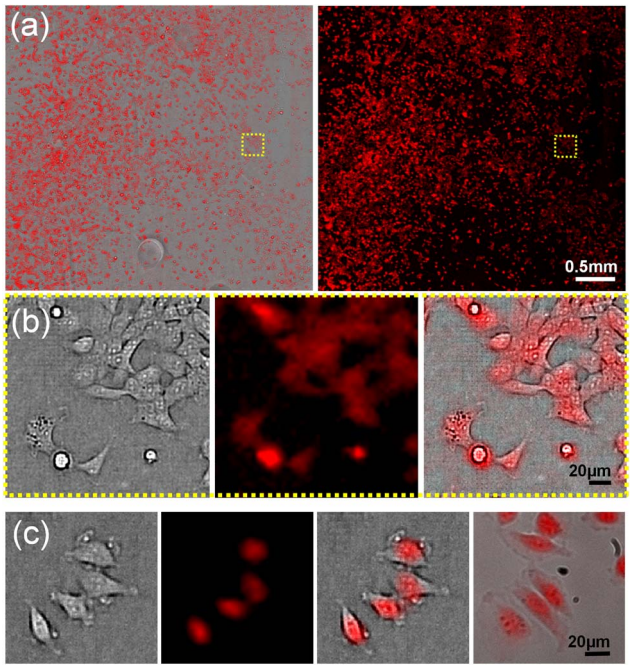

Fig. 3. Bright-field and fluorescence images of living cells taken with a SF sensor chip. (a) Large FOV images of HEK 293-mCherry cells (Media 2). (b) Bright-field, fluorescence, and overlay images of the area highlighted in (a). (c) MCF-7 cells stained with SYTO-64 nucleic acid stain. SF sensor images and a 20× objective microscope image of the same type of cells on a conventional petri dish.

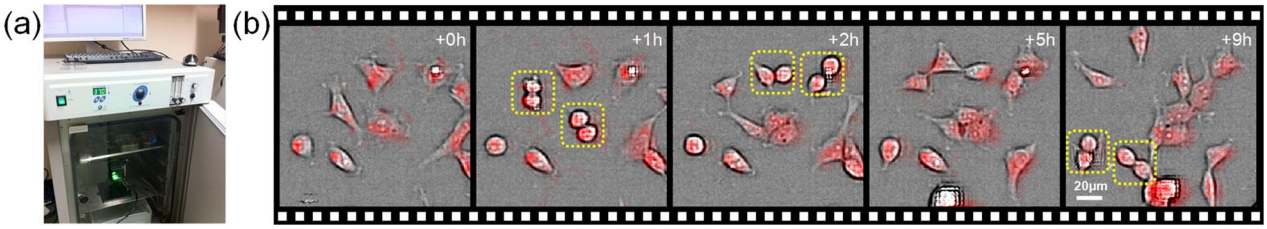

Fig. 4. Long-term monitoring of living cells. (a) A SF-ePetri system is kept in a CO_2 incubator and controlled with a PC. (b) Time-lapse sequence indicating migration and mitosis (boxed) of HEK 293-mCherry cells (Media 3, Media 4, and Media 5).

the UF and SF sensors and imaged with the configuration illustrated in Fig. 1(a). We compared the 8 μm UF with the 6 μm SF to match the background rejection in the images. Figure 2(b) shows the SPSM bright-field and fluorescence images obtained from the UF and SF sensors. 10× objective lens microscope images confirm that the UF and SF sensors can identify fluorescent and nonfluorescent beads. The obtained images demonstrate the improved resolution with the SF, which has confined most of the fluorescence emission to a single pixel or two.

We quantified the resolution limit of the SF sensors with the PSFs obtained in Fig. 2(c). Because the SF pixel is larger than the bead, the location of the bead within the pixel affects the PSF. In the best case, a bead is placed at the center of an SF pixel and the full width at half-maximum (FWHM) measures 1.2 pixels. In the worst case, a bead is placed on the metal grid between two pixels and the FWHM is increased to 2.2 pixels. Based on these measurements, our prototype can resolve two beads that are placed 2.5 pixels (13 μm) apart, regardless of the position of the objects.

Figure 3 shows the images of mammalian cells cultured on an SF ePetri system. We used two types of fluorescently labeled cells: HEK 293 cells expressing mCherry red fluorescent protein (RFP) and MCF-7 cells stained with SYTO-64 red nucleic acid stain. Fluorescence images are taken with a 450 ms exposure. We corrected for the baseline noises resulting from the unblocked excitation light by subtracting the background image taken in the absence of cell samples. The images with the nucleic acid stain can distinguish the cell nucleus from the cytoplasm, whereas RFP-expressing cells fluoresce from all parts of the cells. Although the current fluorescence resolution is insufficient for identifying subcellular structures, image-based biological analyses at single-cell resolution may be applicable when combined with the higher-resolution bright-field images.

The quality of fluorescence images is assessed by computing the signal-to-noise ratio (SNR). Typically, images with more than 30 dB SNR are considered "good" for further analysis. The SNR in each image can be expressed as below:

$$\mathrm{SNR} = 20\log_{10}\left(\frac{\mu_{\mathrm{sig}} - \mu_{\mathrm{bg}}}{\sigma_{\mathrm{bg}}}\right), \quad (1)$$

where μ_{sig} and μ_{bg} are the mean signal and background intensities, respectively, and σ_{bg} is the standard deviation of the background [11]. Background pixels are identified by the inhomogeneity measurement method described in [11]. The computed SNRs of the fluorescent images were 9.5 dB (nucleic acid stain), 32 dB (RFP), and 35 dB (fluorescent beads). Images with nucleic acid stain resulted in relatively low SNR values due to the high background from unbound fluorophores.

Finally, we performed long-term monitoring of cells cultured on an ePetri system using the SF sensors. HEK 293-mCherry cells were grown on a SF-ePetri system placed in the incubator, and a set of bright-field and fluorescence images were obtained at 20 min intervals for 20 h [Fig. 4(b), Media 3–5]. The time-sequence images indicate movement and growth of HEK 293 cells, which suggests that the SF-ePetri system can be adapted for monitoring dynamic processes in biological samples.

In summary, we developed a chip-scale fluorescence microscope using SF-CMOS image sensors. Our extruded pixel design eliminates the undesirable separation between the sample and the CMOS imager that the absorptive filter layer would otherwise introduce. We successfully imaged fluorescent samples with the SF sensor, achieving 13 μm resolution over 4.8 mm × 4.4 mm FOV. In addition, we demonstrated an ePetri imaging system using the SF sensors, which can obtain both bright-field and fluorescence images in a compact, low-cost geometry, suitable for long-term monitoring and various image-based biological analyses.

This project is funded by the NIH under grant 1R01AI096226-01.

References

1. V. Starkuviene and R. Pepperkok, Br. J. Pharmacol. **152**, 62 (2007).
2. T. Schroeder, Nat. Methods **8**, S30 (2011).
3. C.-C. Liang, A. Y. Park, and J.-L. Guan, Nat. Protocols **2**, 329 (2007).
4. X. Cui, L. M. Lee, X. Heng, W. Zhong, P. W. Sternberg, D. Psaltis, and C. Yang, Proc. Natl. Acad. Sci. USA **105**, 10670 (2008).
5. G. Zheng, S. A. Lee, Y. Antebi, M. B. Elowitz, and C. Yang, Proc. Natl. Acad. Sci. USA **108**, 16889 (2011).
6. S. Pang, C. Han, M. Kato, P. W. Sternberg, and C. Yang, Opt. Lett. **37**, 5018 (2012).
7. A. F. Coskun, I. Sencan, T.-W. Su, and A. Ozcan, Analyst **136**, 3512 (2011).
8. A. F. Coskun, I. Sencan, T.-W. Su, and A. Ozcan, Opt. Express **18**, 10510 (2010).
9. S. C. Park, M. K. Park, and M. G. Kang, IEEE Signal Process. Mag. **20**(3), 21 (2003).
10. W. Robert, Proc. Roy. Soc. **59**, 781 (1947).
11. P. Paul, D. Kalamatianos, H. Duessmann, and H. Huber, in *Proceedings of IEEE International Conference on Bio-Informatics and BioEngineering* (IEEE, 2008), pp. 1–6.